

## Article

# Synthesis and Characterization of Cyclodextrin-Based Polyhemiaminal Composites with Enhanced Thermal Stability

Hoque Mohammed Jabelul <sup>1,\*</sup> , Mitsuo Toda <sup>2,\*</sup>  and Nobuyuki Mase <sup>1,2,3</sup> 

<sup>1</sup> Department of Optoelectronics and Nanostructure Science, Graduate School of Science and Technology, Shizuoka University, 3-5-1 Johoku, Hamamatsu 432-8561, Shizuoka, Japan; mase.nobuyuki@shizuoka.ac.jp

<sup>2</sup> Department of Engineering, Graduate School of Integrated Science and Technology, Shizuoka University, 3-5-1 Johoku, Hamamatsu 432-8561, Shizuoka, Japan

<sup>3</sup> Research Institute of Green Science and Technology, Shizuoka University, 3-5-1 Johoku, Hamamatsu 432-8561, Shizuoka, Japan

\* Correspondence: hoque.mohammed.jabelul.15@shizuoka.ac.jp (H.M.J.); toda.mitsuo@shizuoka.ac.jp (M.T.); Tel.: +81-478-1146 (M.T.)

**Abstract:** Polyhemiaminal (PHA) polymers are a new class of thermosetting polymers that have recently gained attention owing to their high mechanical strength and excellent recycling behavior. However, low thermal stability is a common issue in PHA polymers due to the thermally labile crosslinked knots. Herein, crosslinked PHA polymer composites were synthesized by reacting formaldehyde with a precursor solution of 4,4'-oxydianiline (ODA) and cyclodextrins (CDs) ( $\alpha$ -,  $\beta$ -, and  $\gamma$ -). The material obtained under optimal conditions (ODA:CD molar ratio of 1:0.5, 37% aqueous solution of formaldehyde (formalin)) exhibited good film formability and high thermal stability with two characteristic decomposition phenomena and a high char yield. The early decomposition of CDs and char formation led to high thermal stability. Time-resolved NMR analysis was conducted to study hemiaminal bond formation via a condensation reaction between ODA and formaldehyde. Furthermore, PHA matrix formation was confirmed by the dissolution of the deposited CD layer in a solution of *N*-methyl-2-pyrrolidinone containing 8–9 wt.% LiBr at 80 °C and FTIR analysis. Based on the elemental analysis results, PHA network formation was confirmed by considering a single unit of the PHA network with CD composition, including the solvent and water.

**Keywords:** polyhemiaminal; thermal stability; cyclodextrins; composite



**Citation:** Jabelul, H.M.; Toda, M.;

Mase, N. Synthesis and

Characterization of

Cyclodextrin-Based Polyhemiaminal

Composites with Enhanced Thermal

Stability. *Polymers* **2022**, *14*, 1562.

[https://doi.org/10.3390/](https://doi.org/10.3390/polym14081562)

[polym14081562](https://doi.org/10.3390/polym14081562)

Academic Editors: John Vakros,

Evroula Hapeshi, Catia Cannilla and

Giuseppe Bonura

Received: 22 March 2022

Accepted: 4 April 2022

Published: 11 April 2022

**Publisher's Note:** MDPI stays neutral with regard to jurisdictional claims in published maps and institutional affiliations.



**Copyright:** © 2022 by the authors.

Licensee MDPI, Basel, Switzerland.

This article is an open access article

distributed under the terms and

conditions of the Creative Commons

Attribution (CC BY) license ([https://creativecommons.org/licenses/by/](https://creativecommons.org/licenses/by/4.0/)

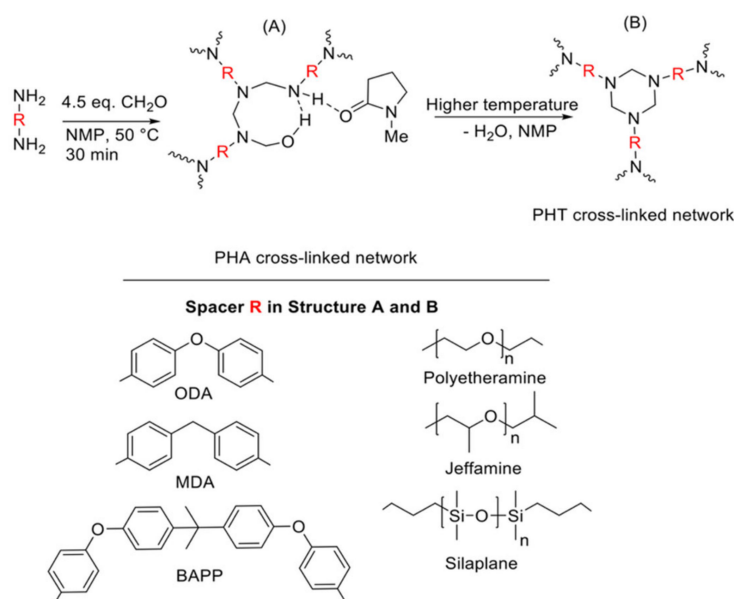
[https://creativecommons.org/licenses/by/](https://creativecommons.org/licenses/by/4.0/)

[4.0/](https://creativecommons.org/licenses/by/4.0/)).

## 1. Introduction

Crosslinked poly(hexahydrotriazine) (PHT) polymers exhibit high mechanical strength, chemical resistance, low density, and pH responsiveness and are consequently attracting increased attention for potential applications in adhesives, coatings, printing materials, and electronic sensors [1–7]. Polymers with triazene or hexahydrotriazine (HT) cores contain photosensitive and thermolabile crosslinks; therefore, they are often used as photopolymers in laser ablation applications [8,9]. Recently, the generation of PHT crosslinks via polyhemiaminal (PHA) intermediate formation at 50 °C followed by cyclization to PHT at 200 °C has been employed to prepare novel thermosetting polymers with an acid-triggered recyclability and good mechanical strength (Young's moduli ~6.3 and ~14 GPa) exceeding those of known thermosets (Scheme 1) [1]. Furthermore, the self-healing properties of organogels intended for adhesive material applications have been probed by computational and experimental model core analyses of supramolecular interaction-based dynamic covalent network formation in PHA [10]. Numerous thermosets have been prepared by copolymerizing reactive species, such as maleimide, epoxides, and acrylates, with PHT or PHA, and characterized in terms of mechanical properties and processability for large-scale applications [11]. Recently, interest has been growing in carbon-fiber-reinforced PHA composites owing to their recyclability, low cost, and ease of fabrication [12–14].

Although these materials exhibit high mechanical strength, recyclability, and self-healing properties, the presence of thermolabile PHT and PHA cores results in insufficient high-temperature performance [7,11]. Generally, thermal properties can be tuned by physically blending various thermoplastic resins or by incorporating reactive species into the reaction mixture to improve homogeneity through chemical modification [11]. In this context, CD/PHA composites were prepared via polycondensation of a precursor solution containing cyclodextrins (CDs) and 4,4'-oxydianiline (ODA) with formaldehyde in *N*-methyl-2-pyrrolidinone (NMP). These cyclic oligomers of glucose exhibit a unique thermal stability range (252–400 °C) and char-forming ability upon degradation [15] and are frequently used as environmentally benign diverse-functionality hosts for suitably sized hydrophobic guests in surfactant and functional polymer applications [16–18]. Although inclusion complexes are formed with hydrophobic guests in water, their implementation in thermosetting polymers is limited by factors such as solvent polarity, reactivity, and solid-state channel structure formation. CD dethreading occurs in polar solvents, whereas the reactivity of the complex is limited in solid-state channel inclusion complexes formed through strong hydrogen bonds [19,20]. In such cases, composite formation can be studied to improve the thermal stability of the PHA polymers. Bio-based natural fiber-reinforced composites are attractive alternatives to those based on glass and carbon fibers in automotive applications owing to their low cost and biodegradability [21,22]. Despite the potential of PHA and PHT crosslink-based polymers, their applications in bio-based natural fiber composites are scarce because of the lack of appropriate functionalization and solubilization procedures for characterization [6,10]. In particular, the synthesis of PHA or PHT-crosslinked polymers with CD composition has not yet been explored. To bridge this gap, we studied CD-based PHA composites and evaluated their thermal properties, solubilities, and recyclabilities. Among the three CDs ( $\alpha$ -,  $\beta$ -, and  $\gamma$ -CDs),  $\alpha$ -CD was preferentially evaluated because it is a readily available low-cost food-grade material. Hemiaminal bond formation before gelation was confirmed using real-time nuclear magnetic resonance (NMR) measurements. The solubility of the obtained polymers was evaluated using NMP/LiBr and dimethylacetamide (DMAc)/LiBr as solvents [23]. As CDs exhibit similar thermal characteristics, this study can be a relevant approach in understanding the formation of PHA-based cellulose composites.



**Scheme 1.** Previously prepared PHA- and PHT-based polymers with variable diamine spacers for thermoset [1], organogel [2], and flexographic plate [3] applications. (A) PHA crosslinked polymer. (B) PHT crosslinked polymer.

## 2. Materials and Methods

### 2.1. Materials

4,4'-oxydianiline (ODA), 4,4'-methylenedianiline (MDA), 2,2-bis(4-(4-aminophenoxy)phenyl)propane (BAPP), and *N,N*-dimethyl-1,4-phenylenediamine (DMPD) were purchased from Tokyo Chemical Industry Co. Ltd. (TCI) (Tokyo, Japan) and had purities of >98%.  $\alpha$ -cyclodextrin ( $\alpha$ -CD) (Food-grade),  $\beta$ -CD,  $\gamma$ -CD, *N*-methyl-2-pyrrolidinone (NMP), and formalin were purchased from Kanto Chemical Co. Inc. (Tokyo, Japan). Paraformaldehyde (PFA) powder (95%) was purchased from Nacalai Chemicals Ltd. (Tokyo, Japan).

### 2.2. Methods

Solid-state Fourier transform infrared FTIR (FT/IR-6300; power = 180 W; working range = 4000–700  $\text{cm}^{-1}$ ; 64 scans; JASCO Corporation, Tokyo, Japan) spectra were recorded at 25 °C. Raman spectra were recorded on a laser spectrometer (NRS-7100; 32 scans, JASCO Corporation, Japan) featuring He-Cd and YAG laser sources with wavelengths of 325, 532, 785, and 1064 nm (600 mW) in the wavenumber range of 3200–100  $\text{cm}^{-1}$ .  $^1\text{H}$  (400.13 MHz) and  $^{13}\text{C}$  (100 MHz) NMR (Avance Ultrashield 400, Bruker Japan, Yokohama, Japan) spectra were recorded using DMSO- $d_6$  as the solvent and tetramethylsilane as an internal standard. Wide-angle X-ray diffraction (XRD) patterns of the powder and solid resin polymer samples were recorded under ambient conditions on a diffractometer (RINT-2200, Rigaku, Tokyo, Japan) equipped with a Cu K ( $\lambda = 1.54 \text{ \AA}$ ) source. Differential scanning calorimetry (DSC) (DSC-60, Shimadzu, Japan) measurements were performed under Ar (25 mL/min) in two temperature ranges (−40 to 40 °C and 40 to 400 °C) at a heating rate of 10 °C/min. Thermogravimetric analysis-differential thermal analysis (TGA-DTA) (DTG-60A, Shimadzu, Kyoto, Japan) measurements were performed under Ar (25 mL/min) in the temperature range of 30–500 °C at a heating rate of 10 °C/min. Field-emission scanning electron microscopy (FE-SEM) imaging was performed on a JSM 6335F instrument (JEOL, Tokyo, Japan) using Au-coated samples to decrease the charge. Atomic force microscopy (AFM) was performed on an AFM VN-8010 instrument (Keyence, Osaka, Japan). Elemental analysis was performed using an elemental analyzer (EA1112, Thermo Electron, Yokohama, Japan).

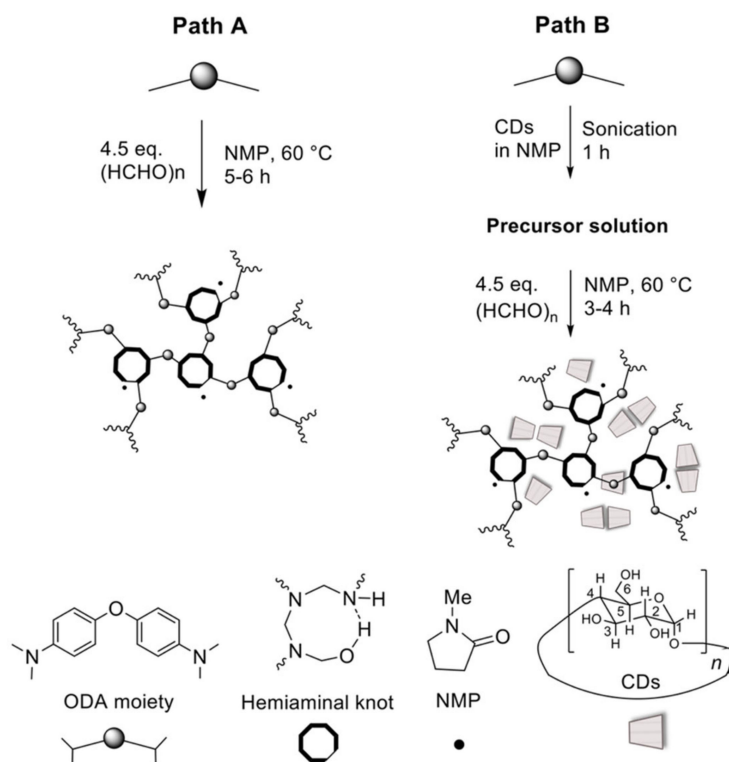
### 2.3. Characterization

To facilitate manipulation and comparative studies, both ODA-PHA (Path A, Scheme 1 [1]) and CDs/ODA-PHA (Path B, Scheme 2, a newly designed process) were synthesized. The reaction conditions are listed in Table 1, and the thermal characteristics and elemental analysis data are listed in Table 2.

**Table 1.** Reaction conditions employed for the synthesis of ODA-PHA and CD/ODA-PHA.

| ODA:CD<br>Molar Ratio | PFA/Formalin<br>eq. vs. ODA <sup>1</sup> | Sonication<br>Time (h) | Reaction<br>Time (h) | Isolated Yield<br>(wt.%) |
|-----------------------|--|------------------------|----------------------|--------------------------|
| 1:0 (ODA)             | 4.5 (PFA)                                | –                      | 24                   | 85–90                    |
| 1:0.5 ( $\alpha$ -CD) | 4.5 (PFA)                                | 1                      | 8–10                 | 85–90                    |
| 1:0.5 ( $\alpha$ -CD) | 4.5 (formalin)                           | 1                      | 2–3                  | 85–90                    |
| 1:0.5 ( $\beta$ -CD)  | 4.5 (formalin)                           | 1                      | 3–4                  | 80–85                    |
| 1:0.5 ( $\gamma$ -CD) | 4.5 (formalin)                           | 1                      | 20–24                | <75                      |

<sup>1</sup> Two different formaldehyde sources (PFA and formalin) were used in the synthesis.



**Scheme 2.** Synthesis of ODA-PHA (Path A) and CDs/ODA-PHA (Path B) via polycondensation of ODA and PFA. Other diamines (MDA and BAPP) were also employed.

**Table 2.** Final  $T_d$ , char yield, and elemental analysis data (based on a hypothetical model) of ODA-PHA and CD/ODA-PHA prepared at an ODA:CD molar ratio of 1:0.5.

| Compound     | $T_d$ (°C) <sup>1</sup> | Char Yield (wt.) <sup>2</sup> | Experimental C/H/N/O Contents (wt.) <sup>3</sup> | Calcd. C/H/N/O Contents (wt.) and Formulas <sup>4</sup>                                  |
|--------------|-------------------------|-------------------------------|--|--|
| ODA-PHA      | 293                     | 65.5                          | 65.9/6.1/11.4/16.6                               | 66.2/6.6/11.9/15.3<br>(C <sub>52</sub> H <sub>62</sub> N <sub>8</sub> O <sub>9</sub> )   |
| α-CD/ODA-PHA | 365                     | 39.8                          | 54.0/6.7/7.1/32.2                                | 55.2/6.4/5.9/32.6<br>(C <sub>88</sub> H <sub>122</sub> N <sub>8</sub> O <sub>39</sub> )  |
| β-CD/ODA-PHA | 366                     | 42.9                          | 55.3/6.8/6.7/31.2                                | 55.3/6.3/5.5/32.9<br>(C <sub>94</sub> H <sub>128</sub> N <sub>8</sub> O <sub>42</sub> )  |
| γ-CD/ODA-PHA | 364                     | 41.1                          | 54.7/6.9/6.2/32.2                                | 54.5/6.3/5.1/34.1<br>(C <sub>100</sub> H <sub>138</sub> N <sub>8</sub> O <sub>47</sub> ) |

<sup>1,2</sup> Determined and calculated from TGA thermograms (Figure S6). <sup>3</sup> Determined from the elemental analysis results. <sup>4</sup> Calculated values based on the molecular formulas listed in the table according to a hypothetical model (Figure S2 and Table S1).

### 2.3.1. Synthesis of ODA-PHA

ODA-PHA was prepared as previously described [1]. Additionally, the respective condensation reactions were performed using formalin as a source of formaldehyde.

### 2.3.2. Synthesis of CD/ODA-PHA

A 100 mL oval-shaped round-bottom flask was charged with ODA (0.20 g, 1.02 mmol, 1.0 eq.), α-CD (0.50 g, 0.51 mmol, 0.5 eq.), and NMP (4.0 mL), and the mixture was sonicated in an ultrasonic bath for 60 min to obtain a clear solution (precursor solution), which was then treated with PFA or formalin (0.14 g, 4.60 mmol, 4.5 eq.). The flask was immersed in an oil bath equipped with a reflux condenser under Ar, and the temperature was slowly raised to 55–60 °C under stirring. Within 1 h, the mixture turned into a viscous liquid

and an opaque gel was obtained after 3–4 h. The obtained product was cooled to 25 °C and mixed with acetone (4 mL). The precipitate was filtered, rinsed with acetone (6–8 mL), and washed with water (8–10 mL) to remove the excess  $\alpha$ -CD. The resulting white waxy resin was vacuum-dried at 50 °C for 8–10 h. The product obtained at 0.83 g corresponded to ~90 wt.% (insoluble fraction), including the solvent trapped in the polymer network.

#### 2.4. NMR Spectroscopic Analysis

$^1\text{H}$  NMR (400 MHz,  $\text{DMSO-}d_6$ ) of ODA-PHA (Figure S1a):  $\delta$  (ppm) 6.73–6.53 (Ar-H), 5.90 (Ar-NH-), 4.72 (-CH<sub>2</sub>-), and 4.42 (-OH).

$^{13}\text{C}$  NMR (100 MHz,  $\text{DMSO-}d_6$ ) (Figure S1b):  $\delta$  (ppm) 149.1 (C<sub>M</sub>), 143.8 (C<sub>N</sub>), 119.4 (C<sub>Q</sub>), and 115.4 (C<sub>P</sub>), 89.9 (-CH<sub>2</sub>-), 84.5 (PFA).

$^1\text{H}$  NMR (400 MHz,  $\text{DMSO-}d_6$ ) of  $\alpha$ -CD/ODA-PHA (Figure S1c):  $\delta$  (ppm) 6.97–6.45 (Ar-H), 6.25 (Ar-NH-), 5.56 (O<sub>2</sub>H), 5.52 (O<sub>3</sub>H), 4.82 (H<sub>1</sub>), 4.69 (-CH<sub>2</sub>-), 4.64 (O<sub>6</sub>H), 4.40 (-OH), 3.73–3.18 (H<sub>5</sub> to H<sub>2</sub>).

$^{13}\text{C}$  NMR (100 MHz,  $\text{DMSO-}d_6$ ) (Figure S1d):  $\delta$  (ppm) 149.1 (C<sub>M</sub>), 144.2 (C<sub>N</sub>), 119.4 (C<sub>P</sub>), 115.6 (C<sub>Q</sub>), 102.4 (C<sub>1</sub>), 89.9 (-CH<sub>2</sub>-), 84.6 (PFA), 82.5 (C<sub>2</sub>), 73.7 (C<sub>3</sub>), 72.5 (C<sub>4</sub> and C<sub>5</sub>), 60.5 (C<sub>6</sub>).

$^1\text{H}$  NMR (400 MHz,  $\text{DMSO-}d_6$ ) of  $\beta$ -CD/ODA-PHA (Figure S1e):  $\delta$  (ppm) 7.01–6.57 (Ar-H), 6.15 (Ar-NH-), 5.75 (O<sub>2</sub>H), 5.69 (O<sub>3</sub>H), 4.84 (H<sub>1</sub>), 4.68 (-CH<sub>2</sub>-), 4.49 (O<sub>6</sub>H), 4.40 (-OH), 3.64–3.25 (H<sub>2</sub> to H<sub>5</sub>).

$^{13}\text{C}$  NMR (100 MHz,  $\text{DMSO-}d_6$ ) (Figure S1f):  $\delta$  (ppm) 149.2 (C<sub>M</sub>), 143.9 (C<sub>N</sub>), 119.4 (C<sub>Q</sub>), 115.7 (C<sub>P</sub>), 102.4 (C<sub>1</sub>), 89.9 (-CH<sub>2</sub>-), 84.5 (PFA), 82.0 (C<sub>2</sub>), 73.5 (C<sub>3</sub>), 72.9 (C<sub>4</sub>), 72.5 (C<sub>5</sub>), 60.4 (C<sub>6</sub>).

$^1\text{H}$  NMR (400 MHz,  $\text{DMSO-}d_6$ ) of  $\gamma$ -CD/ODA-PHA (Figure S1g):  $\delta$  (ppm) 6.69–6.55 (Ar-H), 6.21 (Ar-NH-), 5.79 (O<sub>2</sub>H), 5.76 (O<sub>3</sub>H), 4.89 (H<sub>1</sub>), 4.64 (-CH<sub>2</sub>-), 4.52 (O<sub>6</sub>H), 4.40 (-OH), 3.63–3.33 (H<sub>2</sub> to H<sub>5</sub>).

$^{13}\text{C}$  NMR (100 MHz,  $\text{DMSO-}d_6$ ) (Figure S1h):  $\gamma$ -CD:  $\delta$  (ppm) 149.1 (C<sub>M</sub>), 144.2 (C<sub>N</sub>), 119.4 (C<sub>Q</sub>), 115.5 (C<sub>P</sub>), 102.1 (C<sub>1</sub>), 89.9 (-CH<sub>2</sub>-), 84.5 (PFA), 81.4 (C<sub>2</sub>), 73.4 (C<sub>3</sub>), 73.0 (C<sub>4</sub>), 72.6 (C<sub>5</sub>), 60.4 (C<sub>6</sub>).

#### 2.5. FTIR Analysis

ODA-PHA (Figure 1):  $\nu$  (cm<sup>-1</sup>) = 3373 (O-H), 2918 (C-H), 1678 (C=O of NMP) [24,25], 1497 (C=C) [26], and 1214 (C-N) [27].

$\alpha$ -CD/ODA-PHA:  $\nu$  (cm<sup>-1</sup>) = 3347 (O-H), 2926 (C-H), 1663 (C=O of NMP), 1501 (C=C), 1232 (C-N), 1031 (C-O-C) [28].

#### 2.6. Raman Analysis

ODA-PHA (Figure 2):  $\nu$  (cm<sup>-1</sup>) = 3068 (N-H), 2928 (C-H), 1614 (C=C), 1434 (C-H), 1166 (C-C), and 925 (C-N) [29,30].

CDs/ODA-PHA:  $\nu$  (cm<sup>-1</sup>) = 3070 (N-H), 2930 (C-H), 1613 (C=C), 1437 (C-H), 1168 (C-C), 930 cm<sup>-1</sup> (C-N) [29].

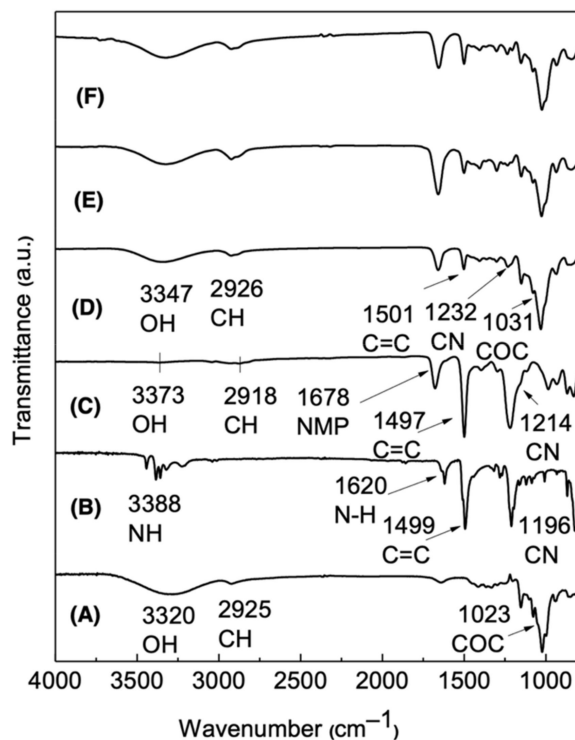


**Figure 1.** FTIR spectra of (A)  $\alpha$ -CD, (B) ODA, (C) ODA-PHA, (D)  $\alpha$ -CD/ODA-PHA, (E)  $\beta$ -CD/ODA-PHA, and (F)  $\gamma$ -CD/ODA-PHA. Among the three CDs,  $\alpha$ -CD was used to compare the band positions of polymer composites.

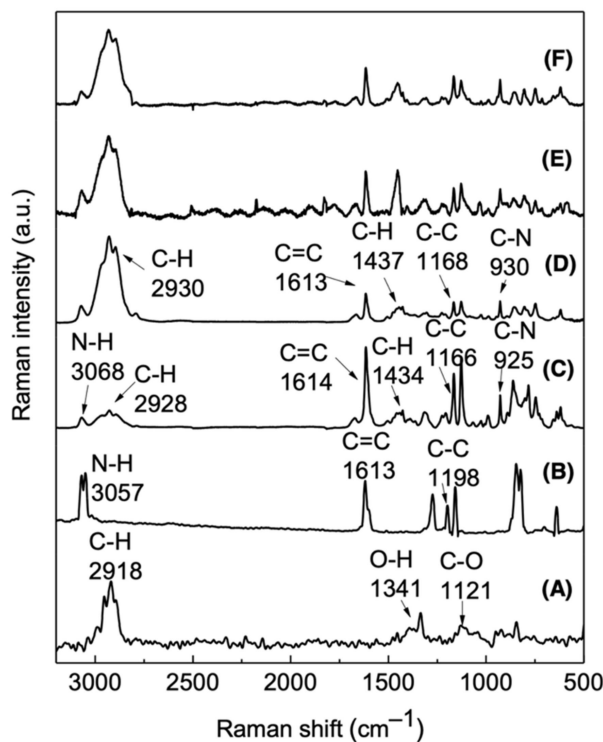


**Figure 2.** Raman spectra of (A)  $\alpha$ -CD, (B) ODA, (C) ODA-PHA, (D)  $\alpha$ -CD/ODA-PHA, (E)  $\beta$ -CD/ODA-PHA, and (F)  $\gamma$ -CD/ODA-PHA.

### 3. Results and Discussion

Considering previous studies on PHA and PHT polymers (Scheme 1), we studied PHA composite formation with three CDs ( $\alpha$ -,  $\beta$ -, and  $\gamma$ -). In this respect, a sonicated precursor solution of monomers (ODA, MDA, and BAPP) was treated with PFA in NMP at 60 °C to obtain CD/PHA. Notably, NMP was reported to form a matrix with  $\beta$ -CD owing to the diffusion of water [31]. Both bulk polymerization and film formation were conducted to understand the matrix-assisted composite formation. The obtained CD/PHA composites were then subjected to thermal, solubility, and recyclability tests. The results showed that, in the presence of CD, aromatic diamines underwent polycondensation with formaldehyde to afford PHA composites. The incorporation of CD resulted in a marked change in the physical state, that is, the final products were obtained as solid resins as opposed to powders (Schemes 2 and S1). Different ODA:CD molar ratios (1:1 and 1:0.5) were used to optimize the properties of the resulting polymers, with the best result obtained at a ratio of 1:0.5. The condensation reactions were carried out according to Scheme 2 (Path A) used to prepare the reference material [1] and (Path B) used to prepare CDs/PHA. The reaction was faster in the case of formalin (Table 1), indicating the promotional effect of water contained in this reagent, in agreement with a previous report [10]. Moreover, although formaldehyde had to be released from PFA by cracking, no such kinetic barrier was present in the case of formalin. The time required to accomplish condensation during heating at 60 °C was determined (based on gelation) to be 3–4 h for the  $\alpha$ -CD-ODA precursor solution. Both ODA-PHA and CD/ODA-PHA films were prepared in formalin by heating on a Petri dish (Scheme S1). The transparent  $\alpha$ -CD-based film exhibited better flexibility than the reference ODA-PHA film did. Moreover, the ODA-PHA film shrank during thermal curing at 60 °C, whereas the  $\alpha$ -CD/ODA-PHA films strongly adhered to the glass surface owing to their adhesive properties. In addition to the spectroscopic assessments, hemiaminal bond formation was confirmed by real-time time-resolved  $^1\text{H}$  NMR analysis at a probe temperature of 55 °C. Furthermore, elemental analysis confirmed the previously proposed formation of a solvent-stabilized PHA core [1] and suggested a component model analysis for both the ODA-PHA polymer and the CD/ODA-PHA composites (Figure S2, Table S1). Finally, both the ODA-PHA polymer and CDs/ODA-PHA composites were recycled by decomposing in 1 N  $\text{H}_2\text{SO}_4$  (aq.) and precipitating in 1 M  $\text{Na}_2\text{CO}_3$  (aq.).

#### 3.1. FTIR Analysis

FTIR spectroscopy was used to analyze the composite formation. As ODA-PHA was formed via a polycondensation reaction, the intensity loss of the amine band ( $\sim 3388\text{ cm}^{-1}$ ) and the emergence of the O–H band ( $\sim 3388\text{ cm}^{-1}$ ) and C–H band ( $\sim 2918\text{ cm}^{-1}$ ) were observed (Figure 1). Two characteristic bands at  $\sim 1497\text{ cm}^{-1}$  and  $\sim 1214\text{ cm}^{-1}$  were observed because of the C=C stretching of the phenyl group and the C–N stretching of either the amine part or the hemiaminal moiety. One extra band at  $\sim 959\text{ cm}^{-1}$  due to C–H bending was observed for ODA-PHA and did not stem from ODA, indicative of hemiaminal core formation. An extra band at  $\sim 1678\text{ cm}^{-1}$  observed even after vacuum drying at 60 °C for 8–12 h was ascribed to the C=O stretching of NMP, as previously reported for Path A synthesis [1]. By contrast, the CD/ODA-PHA composites showed combined bands for both the ODA-PHA core and CD. In addition to the characteristic C=C and C–N stretching bands, typical O–H stretching at  $\sim 3347\text{ cm}^{-1}$  and C–O–C stretching at  $\sim 1031\text{ cm}^{-1}$  were observed. Neither the characteristic amine bands nor an overlap of the O–H and N–H bands was observed for CD/ODA-PHA.

#### 3.2. Raman Analysis

In the Raman spectra of ODA-PHA and CD/ODA-PHA, the characteristic amine band of ODA ( $\sim 3057\text{ cm}^{-1}$ ) disappeared (Figure 2), whereas a C–H band ( $\sim 2928\text{ cm}^{-1}$ ) associated with hemiaminal bond formation appeared. Compared with ODA-PHA, an intense C–H signal ( $\sim 2930\text{ cm}^{-1}$ ) was observed for CDs/ODA-PHA because of the overlap of the C–H bands of CD and hemiaminal bonds. A small sharp peak at  $\sim 3068\text{ cm}^{-1}$ , which

was observed for both polymers and did not stem from  $\alpha$ -CD, was ascribed to N–H (secondary amine) stretching of the hemiaminal linkages. Furthermore, characteristic C=C stretching of the phenyl group at  $\sim 1614\text{ cm}^{-1}$  and C–N stretching of the hemiaminal linkage at  $\sim 925\text{ cm}^{-1}$  were observed for both ODA-PHA and CD/ODA-PHA [29,30]. Notably, the polymer composites exhibited identical but less intense Raman shifts than ODA-PHA within the range of  $1700\text{--}500\text{ cm}^{-1}$ . These results clearly confirmed the formation of CD/PHA composites.

### 3.3. Powder XRD Analysis

No crystalline peaks related to ODA or the CDs were observed in the XRD patterns (Figure 3). The major peak of ODA-PHA appeared as a broad hump at  $\sim 17.9^\circ$ , which was ascribed to the diffusion of scattered incident radiation [1]. By contrast, CD/ODA-PHA exhibited two major CD peaks at  $\sim 20.0^\circ$  and  $\sim 20.1^\circ$ . The significant shift in the major broad peak confirmed that the originally crystalline CD became amorphous upon composite formation [32]. Moreover, for the polymer composites containing  $\alpha$ -,  $\beta$ -, and  $\gamma$ -CD, the signals corresponding to the ODA-PHA matrix shifted to  $13.2^\circ$ ,  $15.4^\circ$ , and  $16.2^\circ$ , respectively, and were less intense than those of ODA-PHA. These results indicated that the polymer composites had an ODA-PHA matrix composed of CDs.

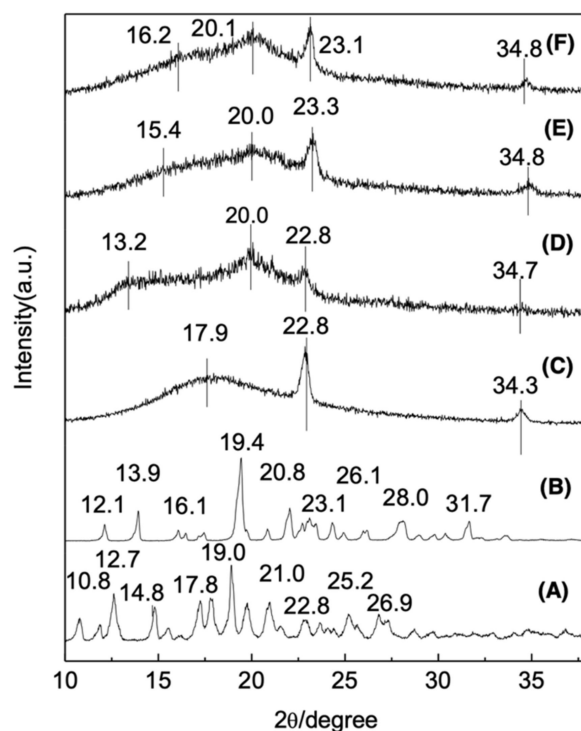


**Figure 3.** XRD patterns of (A)  $\alpha$ -CD, (B) ODA, (C) ODA-PHA, (D)  $\alpha$ -CD/ODA-PHA, (E)  $\beta$ -CD/ODA-PHA, and (F)  $\gamma$ -CD/ODA-PHA.

### 3.4. Hemiaminal Core Studies Using NMR Spectroscopy

Hemiaminal bond formation was monitored via real-time time-resolved  $^1\text{H}$  NMR analysis prior to gel formation at a probe temperature of  $55^\circ\text{C}$  (direct procedure). ODA (0.02 g) was dissolved in  $\text{DMSO-}d_6$ , and the NMR spectrum was recorded after 10 min. Another tube containing ODA (1.0 eq.), PFA (4.5 eq.), and  $\text{DMSO-}d_6$  was immediately analyzed at the starting point. Successive NMR spectra were recorded after each 10 min interval (Figure 4). The hemiaminal bond formation was observed after 10 min, as confirmed by the emergence of new peaks due to hemiaminal protons at 5.87 ppm ( $-\text{NH}-$ ), 4.69 ppm ( $-\text{OH}$ ), and 4.43 ppm ( $-\text{CH}_2-$ ), as well as consumption of PFA peak at 4.83 ppm ( $-\text{CH}_2-$ ). The relative integral values of the hemiaminal peaks increased, whereas those

of the PFA peak increased with respect to time. The molar ratio was calculated based on the relative integral values of the hemiaminal peaks ( $-\text{NH}-$  and  $-\text{OH}$ ) and PFA peaks ( $-\text{CH}_2-$ ), and plotted with respect to time. The molar ratio increased dramatically over time (Figure 4).  $^1\text{H}$  NMR measurements were performed using a model compound (DMPD). The emergence of hemiaminal peaks was observed at 5.30 ppm ( $-\text{NH}-$ ), 4.54 ppm ( $-\text{CH}_2-$ ), and 4.39 ppm ( $-\text{OH}$ ) (Figure S1i). However, a synergistic methylene peak arising from the hemiaminal bond evolved near the methylene protons of the PFA. The integral values of the hemiaminal peaks increased with a decrease in PFA peaks. Composite formation was monitored via NMR measurements at  $55^\circ\text{C}$  by reacting a precursor solution of  $\alpha\text{-CD}$ , ODA, and formalin in  $\text{DMSO-}d_6$ . As the reaction proceeded, some new peaks emerged at 5.98 ppm, 4.70 ppm, and 4.62 ppm due to hemiaminal protons, such as  $-\text{NH}-$ ,  $-\text{CH}_2-$ , and  $-\text{OH}$ , respectively (Figure S1j). Notably, the aromatic and hydroxyl proton peaks of  $\alpha\text{-CD}$  broadened significantly with time owing to gel formation. However, the  $\alpha\text{-CD}$  cavity and anomeric protons remained unchanged for up to 120 min.

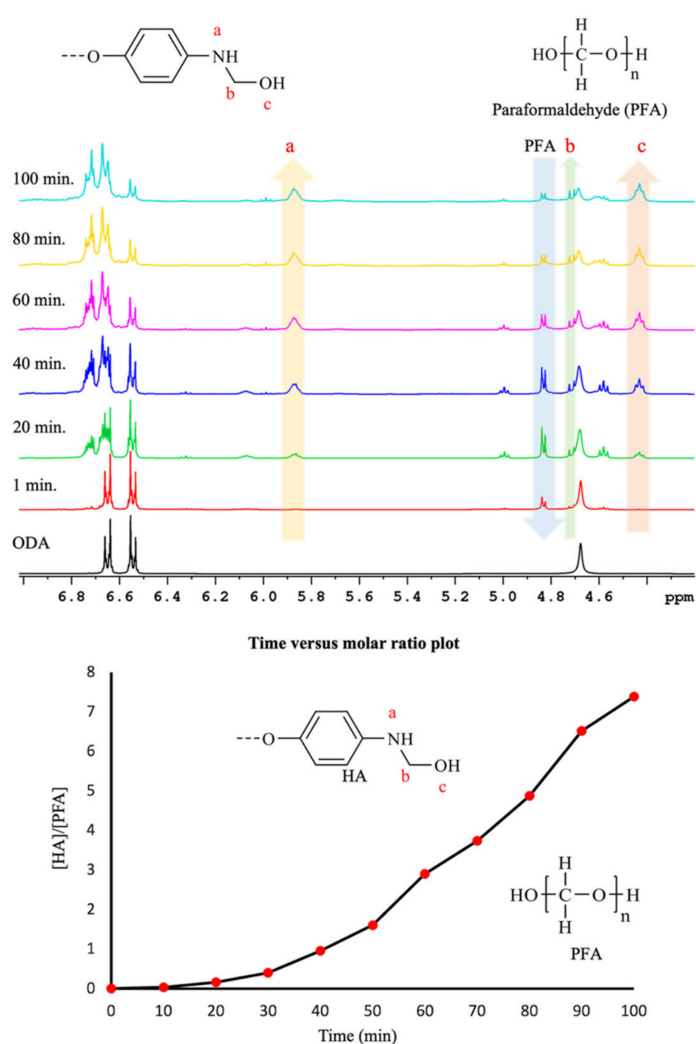


**Figure 4.**  $^1\text{H}$ -NMR spectra of ODA-hemiaminal bond formation at a probe temperature of  $55^\circ\text{C}$  acquired after 10 min intervals up to 100 min. Variation in the molar ratio of hemiaminal and PFA based on relative integral values of  $-\text{NH}-$  protons of hemiaminal bond and  $-\text{CH}_2-$  protons of PFA.

Hemiaminal core formation was monitored indirectly. In this case, the required amounts of diamine and 100% formalin (4.5 eq.) were placed in a small flask, and DMSO- $d_6$  was added instead of NMP. The mixture was then heated to 60 °C for 20 min, and NMR spectra were recorded. In the  $^1\text{H}$  NMR spectra, hemiaminal protons associated with (Ar-NH-),  $-\text{CH}_2-$ , and  $-\text{OH}$  appeared at 5.90 ppm, 4.72 ppm, and 4.42 ppm, respectively (Figure S1a). In the  $^{13}\text{C}$  NMR spectrum, a hemiaminal carbon peak appeared at 89.9 ppm (Figure S1b). To monitor the composite formation, the required amounts of diamine and the CDs were dissolved in DMSO- $d_6$ , followed by sonication (1 h), the addition of formalin (4.5 eq.), and stirring. An aliquot was then transferred to an NMR tube and heated at 60 °C for 20 min. In the  $^1\text{H}$  NMR spectrum of  $\alpha$ -CD/ODA-PHA, hemiaminal protons, such as (Ar-NH-),  $-\text{CH}_2-$ , and  $-\text{OH}$ , were assigned at 6.25 ppm, 4.69 ppm, and 4.40 ppm, respectively. Notably, a hemiaminal carbon resonance peak was observed at the same position as ODA-PHA at 89.9 ppm for all composites.

### 3.5. TGA

In the TGA thermogram, ODA exhibited single-step weight loss (99.0%) associated with two sharp endothermic peaks at 198.6 °C and 346.3 °C (Figures 5 and S3). Similarly, the thermogram of  $\alpha$ -CD showed two major endothermic peaks, with a total weight loss of 99.2%. No characteristic endothermic peaks were observed for either ODA-PHA or CD/ODA-PHA. Typically, ODA-PHA showed two-step weight loss (30.4% and 28.8%) associated with endo- and exothermic peaks. The former was due to solvent and water volatilization, and the latter was related to network degradation. In contrast, thermograms of CD/ODA-PHA exhibited three-step weight loss: 23.3%, 12.6%, and 29.5% for  $\alpha$ -CD/ODA-PHA; 16.7%, 15.3%, and 42.1% for  $\beta$ -CD/ODA-PHA; and 12.5%, 18.5%, and 38.0% for  $\gamma$ -CD/ODA-PHA (Figure 5). The first weight loss was attributed to solvent and water volatilization, whereas the second and third weight losses were attributed to CD decomposition and degradation of aromatic residues, respectively, leading to char formation (Table S2). Notably, the final  $T_d$  significantly increased upon composite formation with CD, which was ascribed to an insulating char barrier formed upon CD decomposition, which slowed the diffusion of oxygen and nitrogen (Figure S3) [15]. The acquired data were used to calculate the char yields at points corresponding to the decomposition of the CDs and the final decomposition of ODA-PHA and CD/ODA-PHA (Table S2). All polymers had almost identical char yields at the final  $T_d$ , with some variations observed only at the first  $T_d$ . The obtained results indicated that the CDs acted as sources of primary char until a stable char was formed at the final  $T_d$ .  $\alpha$ -CD/MDA-PHA and  $\alpha$ -CD/BAPP-PHA were further subjected to TGA to gain insight into the polymer decomposition behavior (Figure S4), which was found to depend on the type of central bond between the two aromatic units (Ar-O-Ar in ODA, Ar- $\text{CH}_2$ -Ar in MDA, and Ar-CMe $_2$ -Ar followed by two ether linkages in BAPP) and on the distance between the two crosslinks [33]. Although BAPP was expected to exhibit the highest bond strength among the three diamines, the presence of two ether linkages next to the aromatic carbons resulted in a bond strength slightly lower than that of MDA. The bond strength decreased in the order MDA > BAPP > ODA, which corresponds to the stability order determined by TGA for the three polymers.

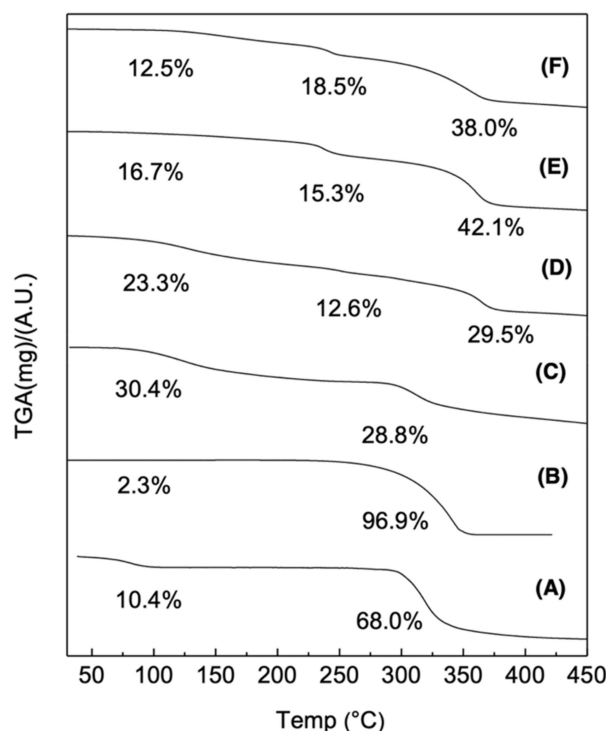


**Figure 5.** TGA thermograms of (A)  $\alpha$ -CD, (B) ODA, (C) ODA-PHA, (D)  $\alpha$ -CD/ODA-PHA, (E)  $\beta$ -CD/ODA-PHA, and (F)  $\gamma$ -CD/ODA-PHA.

### 3.6. DSC

In the DSC thermogram, ODA exhibited a sharp  $T_m$  peak at 195 °C, which evolved into a broad amorphous peak upon polymerization (Figure S5). The  $T_g$  of CD/ODA-PHA decreased in the order  $\alpha$ - >  $\beta$ - >  $\gamma$ -CD, and that of ODA-PHA (107 °C) was similar to the previously reported values. Two major broad exothermic peaks were observed for ODA-PHA and CDs/ODA-PHA. The first exothermic peak and the corresponding enthalpy were determined to be 258 °C and 8.84 J/g for ODA-PHA, 247 °C and 119.8 J/g for  $\alpha$ -CD/ODA-PHA, 241 °C and 74.8 J/g for  $\beta$ -CD/ODA-PHA, and 237 °C and 59.2 J/g for  $\gamma$ -CD/ODA-PHA, respectively. Clearly, the incorporation of CD increased the enthalpy of the first exothermic peak [34]. The enthalpy related to the second exothermic peak at the final decomposition point was determined to be 80.8 J/g for ODA-PHA, 67.4 J/g for  $\alpha$ -CD/ODA-PHA, 106.3 J/g for  $\beta$ -CD/ODA-PHA, and 94.5 J/g for  $\gamma$ -CD/ODA-PHA. DSC analysis conducted from  $-40$  to 40 °C revealed one small transition for ODA-PHA (at  $-4.4$  °C) and  $\alpha$ -CD/ODA-PHA (at  $-7.1$  °C). These peaks, ascribed to the  $T_g$  of these polymers in the low-temperature region, have not been reported previously (Figure S5a). The emergence of exothermic peaks and a shift in the final  $T_d$  value indicated that the CDs improved the thermal stability of the CD/ODA-PHA polymer composites.

### 3.7. Elemental Analysis

Based on the experimental elemental composition data, a hypothetical model was proposed by considering a single unit of the PHA network with the solvent, trapped water, and CD ( $\alpha$ -,  $\beta$ -, or  $\gamma$ -) compositions (Figure S2). The results of the elemental analysis conducted for ODA-PHA and CD/ODA-PHA prepared at ODA:CD molar ratios of 1:1 and 1:0.5 were consistent with the theoretical values determined by considering hypothetical model components (Table 2). Similarly, good agreement was observed between the experimental results and theoretical values for  $\alpha$ -CD/MDA-PHA; however, a slight deviation in the experimental composition was observed for  $\alpha$ -CD/BAPP-PHA, which was ascribed to the different compositions of CD distributed in the composite (Table S1).

The elemental composition was calculated using the following components: ( $X_1$ ) ODA, ( $X_2$ ) hemiaminal, ( $X_3$ ) NMP, (Y) water, and (Z) CD.

### 3.8. FE-SEM

FE-SEM images of the ODA-PHA sample revealed a 3D porous structure [35], whereas those of  $\alpha$ -CD/ODA-PHA showed layered structures with small grooves due to the aggregation of  $\alpha$ -CD in the polymer matrix. (Figure 6).

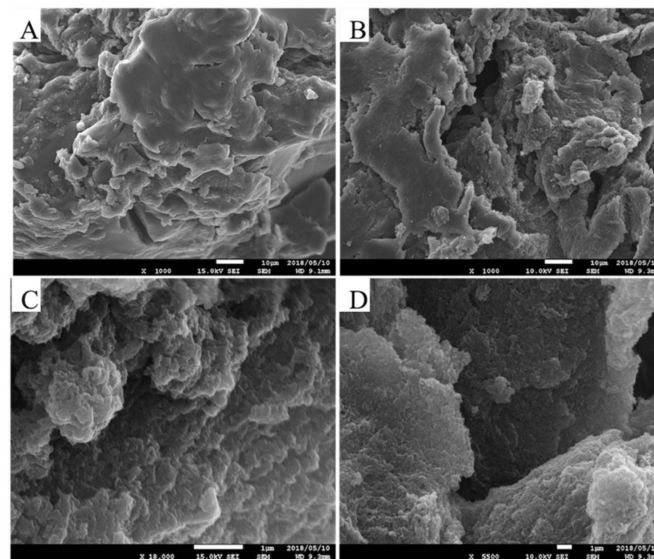


**Figure 6.** FE-SEM images of (A,B)  $\alpha$ -CD/ODA-PHA and (C,D) ODA-PHA.

### 3.9. AFM

AFM analysis revealed a smooth surface for the  $\alpha$ -CD/ODA-PHA film, whereas a rougher surface was observed for the ODA-PHA film (Figure 7). The surface smoothness could be attributed to a layer of  $\alpha$ -CD composited on the ODA-PHA rough surface in  $\alpha$ -CD/ODA-PHA.

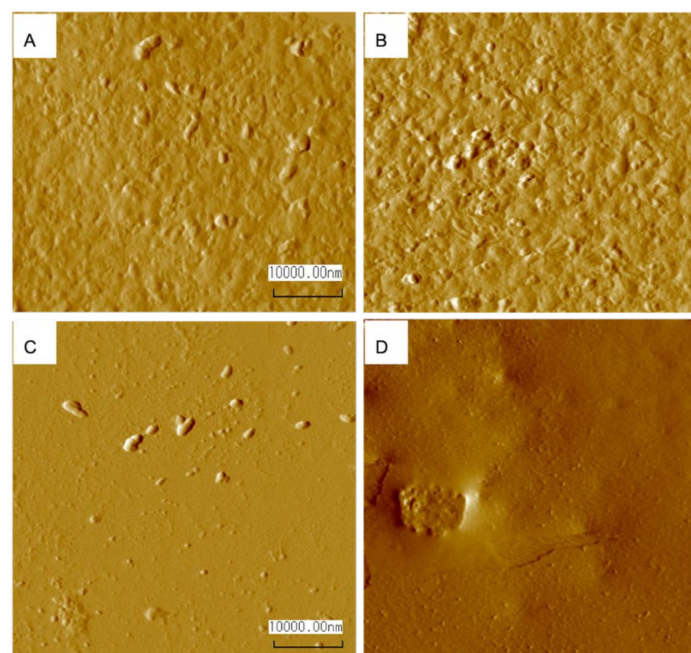


**Figure 7.** AFM images of ODA-PHA (A,B) and  $\alpha$ -CD/ODA-PHA (C,D) films prepared at 60 °C.

### 3.10. Solubility Assay of ODA-PHA and CD/ODA-PHA in NMP/LiBr

DMAC/LiCl and DMAC/LiBr with salt contents of 8–9 wt.% were used as alternative solvents to solubilize polyrotaxanes and facilitate their acetylation and dansylation [23]. The low solubility of polyrotaxanes is due to intra- and intermolecular hydrogen bonding between hydroxyl groups [17,23]. However, these solvents destroy the hydrogen bonds through ionization. In this study, NMP/LiBr and DMAC/LiBr were employed to evaluate the solubilities of ODA-PHA and CDs/ODA-PHA. The maximum proportion of CD/ODA-PHA films (<68 wt.% of initial weight) was dissolved in the NMP/LiBr mixture (8–9 wt.% LiBr) at 80–90 °C in 3–5 h, and the remaining undissolved film was collected for FTIR analysis. By contrast, the ODA-PHA film remained unaffected at this temperature even when the treatment was continued for >72 h. A soluble portion of CD/ODA-PHA films was precipitated in water, filtered, washed with methanol, and vacuum-dried for 24 h. Notably, its FTIR spectrum featured all characteristic bands of  $\alpha$ -CD/ODA-PHA, indicating oligomers of ODA-PHA and  $\alpha$ -CD (Figure S6). The undissolved portion of the  $\alpha$ -CD/ODA-PHA film was washed with water and methanol several times, kept in methanol for 24 h, and vacuum-dried at 60 °C for 3–4 h. The FTIR spectra of the undissolved portion showed characteristic hemiaminal bands such as 2913, 1498, and 1202  $\text{cm}^{-1}$  for C–H, C=C, and C–N stretching, respectively, confirming the formation of the ODA-PHA matrix (Figure S6a).

### 3.11. Diamine Recovery Test

A diamine recovery test was performed by digesting the  $\alpha$ -CD/ODA-PHA composite in 1 N  $\text{H}_2\text{SO}_4$ , followed by precipitation in 1 M  $\text{Na}_2\text{CO}_3$ . Approximately 0.2 g of the composite was placed in a vial, to which 1 N  $\text{H}_2\text{SO}_4$  (6 mL) was added. The polymer was disintegrated within 5 min to obtain a clear solution. When 1 M  $\text{Na}_2\text{CO}_3$  solution was added dropwise,  $\text{CO}_2$  bubbling was observed, along with an increase in pH and the appearance of precipitates. After maintaining a pH of approximately 7–8, precipitation was complete, and bubbling was stopped. The precipitates were filtered and washed with excess hot water to remove CD, which was collected after vacuum drying. The FTIR and NMR spectra of the precipitate were recorded and compared with those of the pristine ODA (Figures S7 and S8). In the FTIR spectrum, the characteristic C=C stretching of the phenyl group ( $\sim 1696 \text{ cm}^{-1}$ ) and C–N stretching ( $\sim 1214 \text{ cm}^{-1}$ ) were observed. The characteristic peaks of the hemiaminal protons were absent in the  $^1\text{H}$  NMR spectrum, indicating ODA recovery.

## 4. Conclusions

In this study, the formation of CD/PHA composites was investigated, revealing that the incorporation of CD resulted in high thermal stability and the emergence of two decomposition phenomena. The early-stage decomposition of the CDs formed a char barrier that improved the thermal stability of the PHA composites. The adopted catalyst-free simple synthesis approach employed readily available chemicals such as food-grade  $\alpha$ -CD, formalin, and a simple aromatic diamine, and is, therefore, suitable for industrial applications. The introduction of CDs through high-throughput synthesis may potentially reduce material costs, and the nontoxicity and environmental friendliness of CDs coupled with the acid-triggered recyclability of PHA polymers make the developed process environmentally viable. The early-stage decomposition of the CDs combined with the thermolabile PHA knot makes the prepared compound a potential component of flexographic materials for laser engraving. Previous laser ablation studies employed various aliphatic polyether diamine-based PHT polymers with 10–20 wt.% carbon black to obtain flexible polymers [3]. The CD/PHA composites prepared herein exhibited inherent flexibility and could act as a carbon source for laser ablation studies. Finally, this study can also be related to the formation of PHA-based cellulosic composites.

**Supplementary Materials:** The following supporting information can be downloaded from <https://www.mdpi.com/article/10.3390/polym14081562/s1>, Supplementary File S1: Synthesis scheme and characterization figures (Scheme S1, Figures S1a–S8, Tables S1 and S2).

**Author Contributions:** Conceptualization, H.M.J., M.T. and N.M.; methodology, H.M.J. and M.T.; software, H.M.J.; validation, H.M.J., M.T. and N.M.; formal analysis, H.M.J.; investigation, H.M.J., M.T. and N.M.; resources, H.M.J., M.T. and N.M.; data curation, H.M.J., M.T. and N.M.; writing—original draft preparation: H.M.J.; writing—review and editing, H.M.J., M.T. and N.M.; visualization, H.M.J.; supervision, M.T. and N.M.; project administration, H.M.J., M.T. and N.M.; funding acquisition, M.T. and N.M. All authors have read and agreed to the published version of the manuscript.

**Funding:** This study received no external funding.

**Institutional Review Board Statement:** Not applicable.

**Acknowledgments:** All major analyses were performed at Shizuoka University Center for Innovation Science. We thank the director of this center and its technical staff, including Ishikawa Makoto, Kusanagi, Aki Miyake and Hayakawa Toshihiro, for their technical support with the analysis. We are also grateful to Kohei Sato and Tetsuya Suzuki for their intellectual support during all stages of this study.

**Conflicts of Interest:** The authors declare no conflict of interest.

## References

1. García, J.M.; Jones, G.O.; Virwani, K.; McCloskey, B.D.; Boday, D.J.; ter Huurne, G.M.; Horn, H.W.; Coady, D.J.; Bintaleb, A.M.; Alabdulrahman, A.M.S.; et al. Recyclable, strong thermosets and organogels via paraformaldehyde condensation with diamines. *Science* **2014**, *344*, 732–735.
2. Fox, C.H.; ter Huurne, G.M.; Wojtecki, R.J.; Jones, G.O.; Horn, H.W.; Meijer, E.W.; Frank, C.W.; Hedrick, J.L.; García, J.M. Supramolecular motifs in dynamic covalent PEG-hemiaminal organogels. *Nat. Commun.* **2015**, *6*, 1–8. [[CrossRef](#)]
3. Hiller, M.; Evsyukov, S.E. Laser-engrivable hexahydrotriazine polymer networks. *Mater. Res. Innov.* **2002**, *6*, 179–184. [[CrossRef](#)]
4. Lippert, T.; Dickinson, J.T. Chemical and spectroscopic aspects of polymer ablation: Special features and novel directions. *Chem. Rev.* **2003**, *103*, 453–485. [[CrossRef](#)]
5. Lippert, T.; Hauer, M.; Phipps, C.R.; Wokaun, A. Fundamentals and applications of polymers designed for laser ablation. *Appl. Phys. A Mater. Sci. Process.* **2003**, *77*, 259–264. [[CrossRef](#)]
6. Kaminker, R.; Callaway, E.B.; Dolinski, N.D.; Barbon, S.M.; Shibata, M.; Wang, H.; Hu, J.; Hawker, C.J. Solvent-free synthesis of high-performance polyhexahydrotriazine (PHT) thermosets. *Chem. Mater.* **2018**, *30*, 8352–8358. [[CrossRef](#)]
7. You, S.; Ma, S.; Dai, J.; Jia, Z.; Liu, X.; Zhu, J. Hexahydro-s-triazine: A trial for acid-degradable epoxy resins with high performance. *ACS Sustain. Chem. Eng.* **2017**, *5*, 4683–4689. [[CrossRef](#)]
8. Kappes, R.S.; Schönfeld, F.; Li, C.; Golriz, A.A.; Nagel, M.; Lippert, T.; Butt, H.J.; Gutmann, J.S. A study of photothermal laser ablation of various polymers on microsecond time scales. *Springerplus* **2014**, *3*, 1–15. [[CrossRef](#)]
9. Lippert, B.T.; Yabe, A.; Wokaun, A. Laser ablation of doped polymer systems. *Adv. Mater.* **1997**, *9*, 105–119. [[CrossRef](#)]
10. Jones, G.O.; García, J.M.; Horn, H.W.; Hedrick, J.L. Computational and experimental studies on the mechanism of formation of poly(hexahydrotriazine)s and poly(hemiaminal)s from the reactions of amines with formaldehyde. *Org. Lett.* **2014**, *16*, 5502–5505. [[CrossRef](#)]
11. Fevre, M.; Wojtecki, R.J.; Hedrick, J.; García, J.M.; Hedrick, J.L. Tailorable thermal properties through reactive blending using orthogonal chemistries and layer-by-layer deposition of poly(1,3,5-hexahydro-1,3,5-triazine) networks. *Adv. Funct. Mater.* **2016**, *26*, 5560–5568. [[CrossRef](#)]
12. Yuan, Y.; Sun, Y.; Yan, S.; Zhao, J.; Liu, S.; Zhang, M.; Zheng, X.; Jia, L. Multiply fully recyclable carbon fibre reinforced heat-resistant covalent thermosetting advanced composites. *Nat. Commun.* **2017**, *8*, 1–11. [[CrossRef](#)] [[PubMed](#)]
13. Lin, Z.; Jia, X.; Yang, J.; Li, Y.; Song, H. Interfacial modification and tribological properties of carbon fiber grafted by TiO<sub>2</sub> nanorods reinforced novel depolymerized thermosetting composites. *Compos. Part A Appl. Sci. Manuf.* **2020**, *133*, 1–11. [[CrossRef](#)]
14. Xu, N.; Kim, S.; Liu, Y.; Adrar, Y.A.; Li, Z.; Hu, Z.; Liu, L.; Hu, Z.; Huang, Y. Facile preparation of rapidly recyclable tough thermosetting composites via crosslinking structure regulation. *Polymer* **2020**, *189*, 1–7. [[CrossRef](#)]
15. Trotta, F.; Zanetti, M.; Camino, G. Thermal degradation of cyclodextrins. *Polym. Degrad. Stab.* **2000**, *69*, 373–379. [[CrossRef](#)]
16. Harada, A.; Takashima, Y.; Nakahata, M. Supramolecular polymeric materials via cyclodextrin-guest interactions. *Acc. Chem. Res.* **2014**, *47*, 2128–2140. [[CrossRef](#)]
17. Wenz, G.; Han, B.H.; Müller, A. Cyclodextrin rotaxanes and polyrotaxanes. *Chem. Rev.* **2006**, *106*, 782–817. [[CrossRef](#)]
18. Takata, T.; Aoki, D. Topology-transformable polymers: Linear-branched polymer structural transformation via the mechanical linking of polymer chains. *Polym. J.* **2018**, *50*, 127–147. [[CrossRef](#)]
19. Wenz, G.; Steinbrunn, M.B.; Landfester, K. Solid state polycondensation within cyclodextrin channels leading to water soluble polyamide rotaxanes. *Tetrahedron* **1997**, *53*, 15575–15592. [[CrossRef](#)]
20. Yang, J.Y.; Te Jung, B.; Suh, D.H. A simple attempt to change the solubility of polyimide by physical inclusion with  $\beta$ -cyclodextrin and its derivatives. *Polymer* **2001**, *42*, 8349–8354. [[CrossRef](#)]
21. Sarker, F.; Karim, N.; Afroj, S.; Koncherry, V.; Novoselov, K.S.; Potluri, P. Ultrahigh Performance of Nanoengineered Graphene-Based Natural Jute Fiber Composites. *ACS Appl. Mater. Interfaces* **2019**, *11*, 21166–21176. [[CrossRef](#)]

22. Sarker, F.; Potluri, P.; Afroj, S.; Koncherry, V.; Novoselov, K.S.; Karim, N. High-performance graphene-based natural fiber composites. *ACS Appl. Mater. Interfaces* **2018**, *10*, 34502–34512. [[CrossRef](#)] [[PubMed](#)]
23. Araki, J.; Ito, K. New solvent for polyrotaxane. I. Dimethylacetamide/lithium chloride (DMAc/LiCl) system for modification of polyrotaxane. *J. Polym. Sci. Part A Polym. Chem.* **2006**, *44*, 532–538. [[CrossRef](#)]
24. Bouziti, H.; Stiti, M.; Abdaoui, M. Spectroscopic and molecular modelling investigations of supramolecular complex of  $\beta$ -cyclodextrin with N-[(4-sulfonamidophenyl) ethyl]-5-(1, 2-dithiolan-3-yl) pentanamide. *J. Incl. Phenom. Macrocycl. Chem.* **2016**, *86*, 121–134. [[CrossRef](#)]
25. Agag, T.; Takeichi, T. Synthesis and characterization of novel benzoxazine monomers containing allyl groups and their high-performance thermosets. *Macromolecules* **2003**, *36*, 6010–6017. [[CrossRef](#)]
26. Tang, X.Z.; Li, W.; Yu, Z.Z.; Rafiee, M.A.; Rafiee, J.; Yavari, F.; Koratkar, N. Enhanced thermal stability in graphene oxide covalently functionalized with 2-amino-4, 6-didodecylamino-1, 3,5-triazine. *Carbon* **2011**, *49*, 1258–1265. [[CrossRef](#)]
27. Sivakumar, K.; Parinamachivayam, G.; Murali Krishnan, M.; Chakravarty, S.; Bharathi, A. Preparation, characterization and molecular modeling studies of the beta-cyclodextrin inclusion complex with benzoguanamine and its analytical application as chemosensor for the selective sensing of Ce<sup>4+</sup>. *Spectrochim. Acta Part A* **2018**, *200*, 212–225. [[CrossRef](#)]
28. Rusa, C.C.; Luca, C.; Tonelli, A.E. Polymer-cyclodextrin inclusion compounds: Toward new aspects of their inclusion mechanism. *Macromolecules* **2001**, *34*, 1318–1322. [[CrossRef](#)]
29. Ghiorghiasa, R.; Petrovici, A.R.; Rosca, I.; Miron, L. Inclusion complex of thiotriazinone with  $\alpha$ -cyclodextrin-Raman spectroscopy, DSC, preliminary antimicrobial and antifungal study. *Dig. J. Nanomater. Bios.* **2016**, *11*, 235–241.
30. Sano, H.; Ichi, T.; Kumashiro, Y.; Kontani, K.; Kuze, T.; Mizutani, G.; Ooya, T.; Yui, N. Raman scattering study of water clusters around polyrotaxane and pseudopolyrotaxane supramolecular assemblies. *Spectrochim. Acta Part A* **2003**, *59*, 285–289. [[CrossRef](#)]
31. Thurein, S.M.; Lertsuphotvanit, N.; Phaechamud, T. Physicochemical properties of  $\beta$ -cyclodextrin solutions and precipitates prepared from injectable vehicles. *Asian J. Pharm. Sci.* **2018**, *5*, 438–449. [[CrossRef](#)]
32. Wang, J.; Wang, P.J.; Gao, P.; Jiang, L.; Li, S.; Feng, Z.G. Distinguishing channel-type crystal structure from dispersed structure in  $\beta$ -cyclodextrin based polyrotaxanes via FTIR spectroscopy. *Front. Mater. Sci.* **2011**, *5*, 329–334. [[CrossRef](#)]
33. Lin, C.H.; Chang, S.L.; Shen, T.Y.; Shih, Y.S.; Lin, H.T.; Wang, C.F. Flexible polybenzoxazine thermosets with high glass transition temperatures and low surface free energies. *Polym. Chem.* **2012**, *3*, 935–945. [[CrossRef](#)]
34. Haynes, A.; Halpert, P.; Levine, M. Colorimetric Detection of Aliphatic Alcohols in  $\beta$ -Cyclodextrin Solutions. *ACS Omega* **2019**, *4*, 18361–18369. [[CrossRef](#)] [[PubMed](#)]
35. Liu, Y.; Zhao, Y.L.; Zhang, H.Y.; Li, X.Y.; Liang, P.; Zhang, X.Z.; Xu, J.J. Supramolecular polypseudorotaxane with conjugated polyazomethine prepared directly from two inclusion complexes of  $\beta$ -cyclodextrin with tolidine and phthaldehyde. *Macromolecules* **2004**, *37*, 6362–6369. [[CrossRef](#)]